

This ESI for *J. Mater. Chem. A*, 2019, 7, 621-631, originally published on 5th December 2018, was updated on 19th February 2020, to fix formatting errors in the uncertainties listed in the legend of Fig. S1.

Carrier density control in $\text{Cu}_2\text{HgGeTe}_4$ and discovery of Hg_2GeTe_4 via phase boundary mapping

Brenden R. Ortiz,^{*,†} Kiarash Gordiz,[†] Lídia C. Gomes,^{‡,¶} Tara Braden,[†] Jesse M.
Adamczyk,[†] Jiaying Qu,^{‡,¶} Elif Ertekin,^{‡,¶} and Eric S. Toberer^{*,†}

[†]*Colorado School of Mines, Golden, Colorado 80401, United States*

[‡]*University of Illinois at Urbana-Champaign, Urbana, Illinois 61801, United States*

[¶]*National Center for Supercomputing Applications, Urbana, Illinois 61801, United States*

E-mail: ortiz.brendenr@gmail.com; etoberer@mines.edu

Electronic Supplementary Information

In this supplementary section, we provide additional X-ray diffraction, microscopy, and transport data to augment the results provided within the main body of “Carrier density control in $\text{Cu}_2\text{HgGeTe}_4$ and discovery of Hg_2GeTe_4 via phase boundary mapping.”

Table S1: Table summarizing some computational predictions for n-type and p-type behavior of the $\text{Cu}_2\text{II}_B\text{IVTe}_4$ diamond-like semiconductors (II_B : Zn, Cd, Hg)(IV: Si, Ge, Sn). This work has been presented in an agglomerate form previously and is available online on our open-source website TEDesignLab.org – it is summarized here for convenience only. We can see that the improved electronic mobility for the n-type predictions leads to significantly higher quality-factor, β , for the n-type compositions.

Compound	β_n	β_p	κ (W/mK)	μ_n (cm^2/Vs)	μ_p (cm^2/Vs)	$m_{b,n}^*$ (m_e)	$m_{b,p}^*$ (m_e)
$\text{Cu}_2\text{ZnSiTe}_4$	18	4	6.9	680	34	0.04	0.33
$\text{Cu}_2\text{ZnGeTe}_4$	19	7	6.5	730	53	0.04	0.24
$\text{Cu}_2\text{ZnSnTe}_4$	19	6	6.0	670	35	0.04	0.30
$\text{Cu}_2\text{CdSiTe}_4$	30	5	6.5	2350	22	0.02	0.42
$\text{Cu}_2\text{CdGeTe}_4$	24	5	6.1	1190	25	0.03	0.38
$\text{Cu}_2\text{CdSnTe}_4$	41	5	6.6	5420	25	0.01	0.39
$\text{Cu}_2\text{HgSiTe}_4$	31	5	6.2	2130	26	0.02	0.38
$\text{Cu}_2\text{HgGeTe}_4$	37	6	5.9	3050	28	0.02	0.35
$\text{Cu}_2\text{HgSnTe}_4$	57	6	5.5	8390	29	0.01	0.33

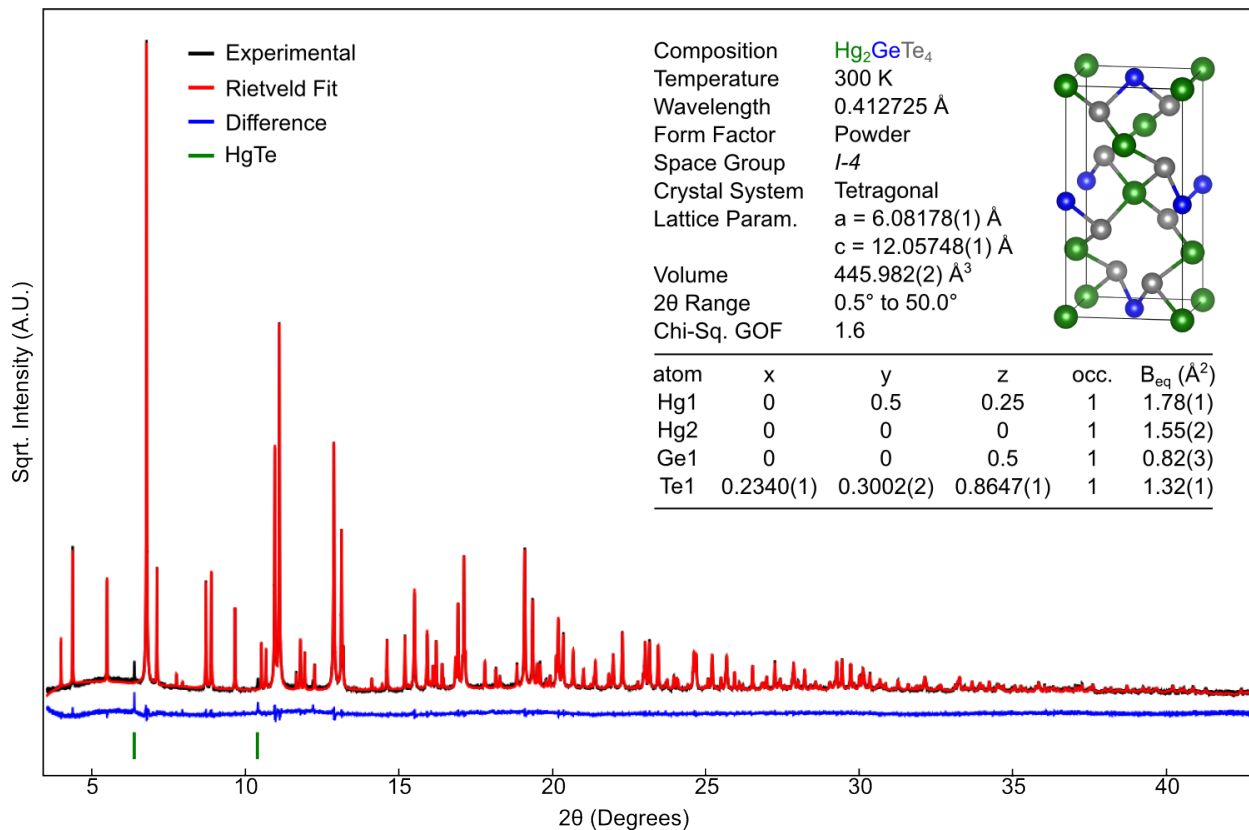


Figure S1: Room-temperature powder synchrotron data (black) was used to solve the crystal structure of Hg_2GeTe_4 (inset) *via* charge flipping methods. Also shown is the subsequent Rietveld refinement (red), the difference profile (blue), and the key crystallographic parameters obtained from the fit. Hg_2GeTe_4 adopts the ordered-vacancy (defect chalcopyrite) structure.

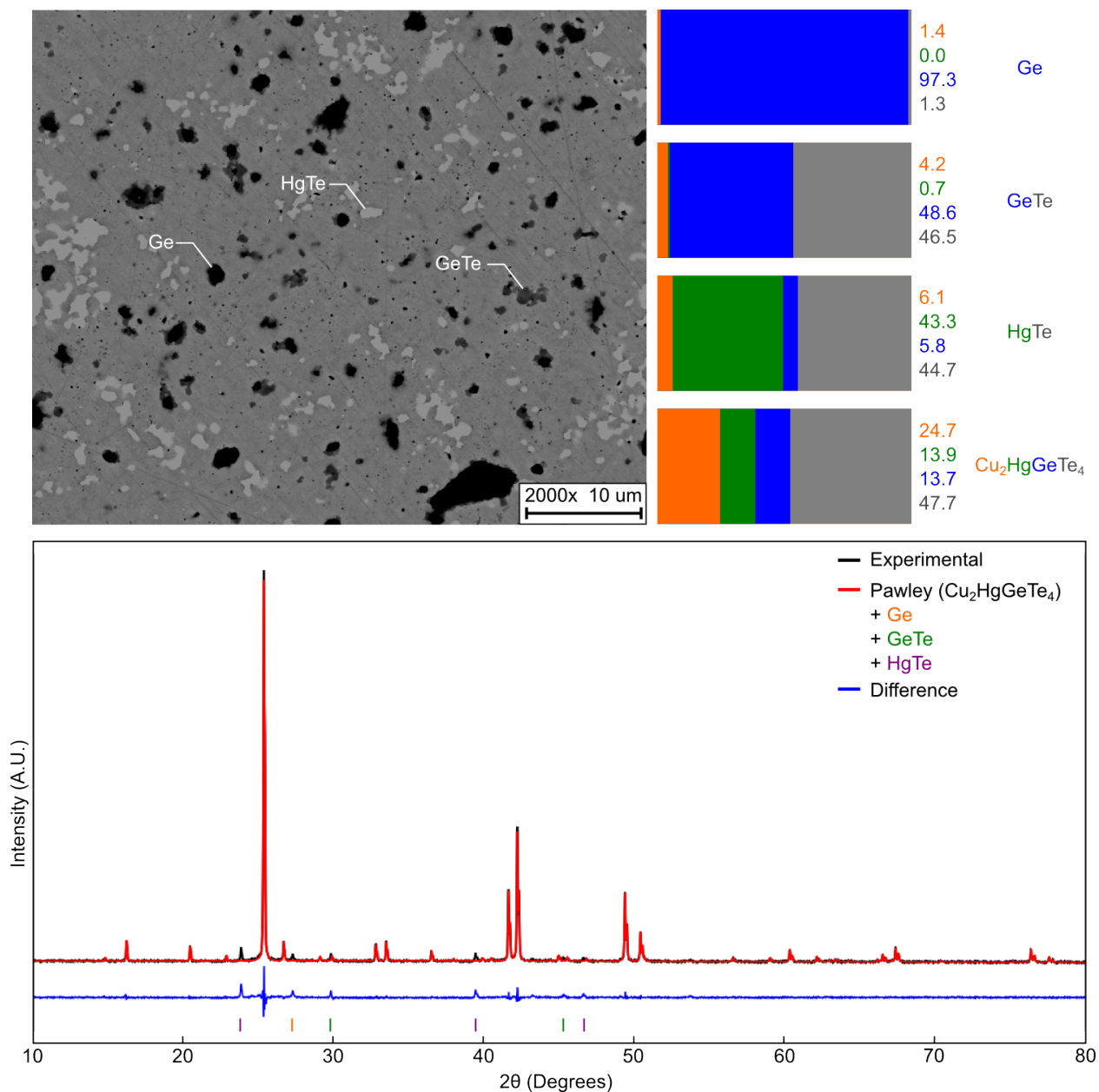


Figure S2: X-ray diffraction (XRD), scanning electron microscopy (SEM), and energy dispersive spectroscopy (EDS) characterization for the Ge-GeTe-HgTe-Cu₂HgGeTe₄ critical point. For XRD, a Pawley analysis is performed to assess the lattice parameters of the Cu₂HgGeTe₄ matrix phase. SEM image is a typical backscatter electron image of the densified pellet. The EDS analysis represents an average composition for each of the impurity phases and the Cu₂HgGeTe₄ matrix phase. EDS was performed and averaged over multiple precipitates (~5) for impurities and multiple locations within the matrix phase (~10).

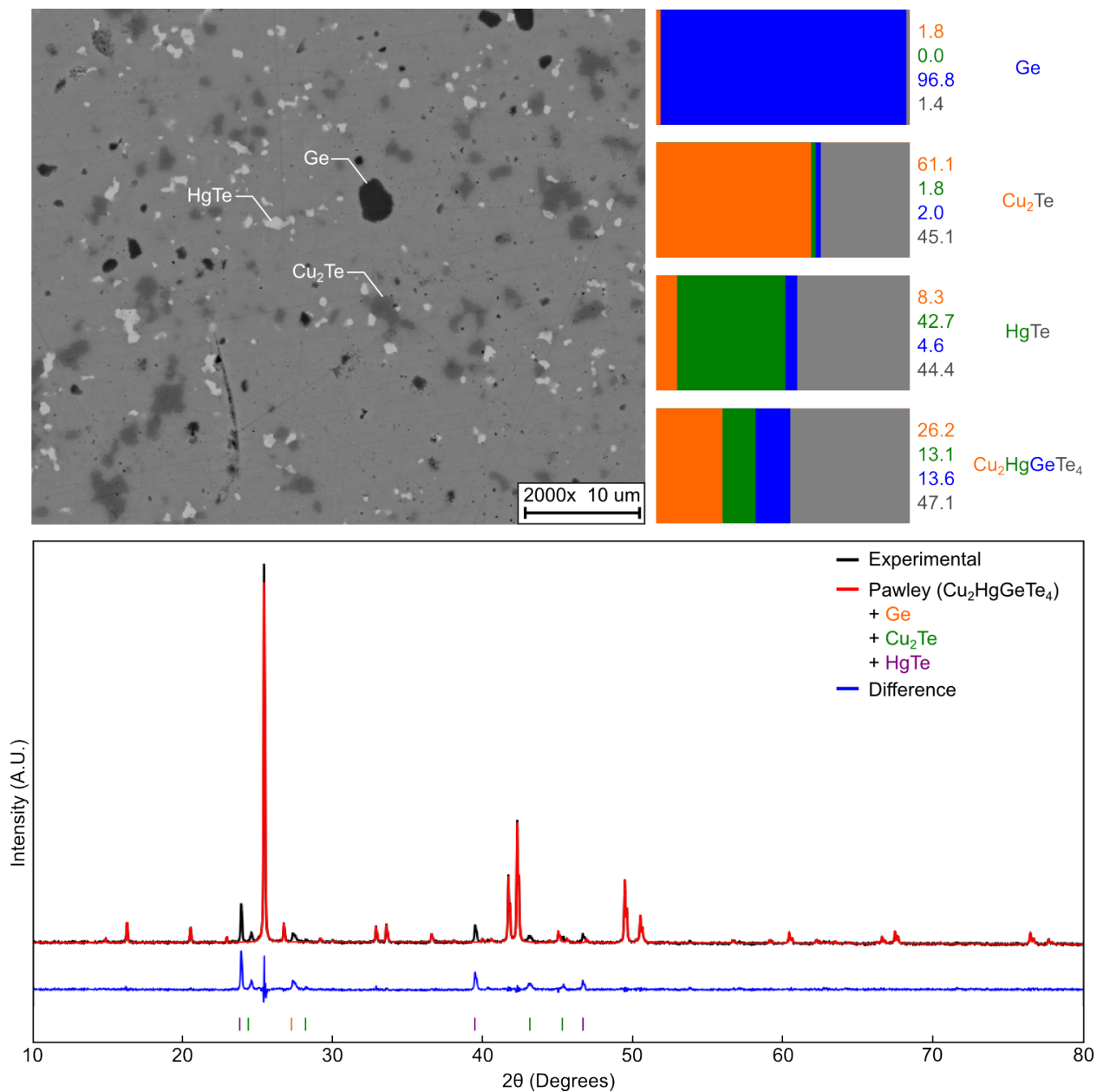


Figure S3: X-ray diffraction (XRD), scanning electron microscopy (SEM), and energy dispersive spectroscopy (EDS) characterization for the Ge- Cu_2Te -HgTe- $\text{Cu}_2\text{HgGeTe}_4$ critical point. For XRD, a Pawley analysis is performed to assess the lattice parameters of the $\text{Cu}_2\text{HgGeTe}_4$ matrix phase. SEM image is a typical backscatter electron image of the den-sified pellet. The EDS analysis represents an average composition for each of the impurity phases and the $\text{Cu}_2\text{HgGeTe}_4$ matrix phase. EDS was performed and averaged over multiple precipitates (~ 5) for impurities and multiple locations within the matrix phase (~ 10).

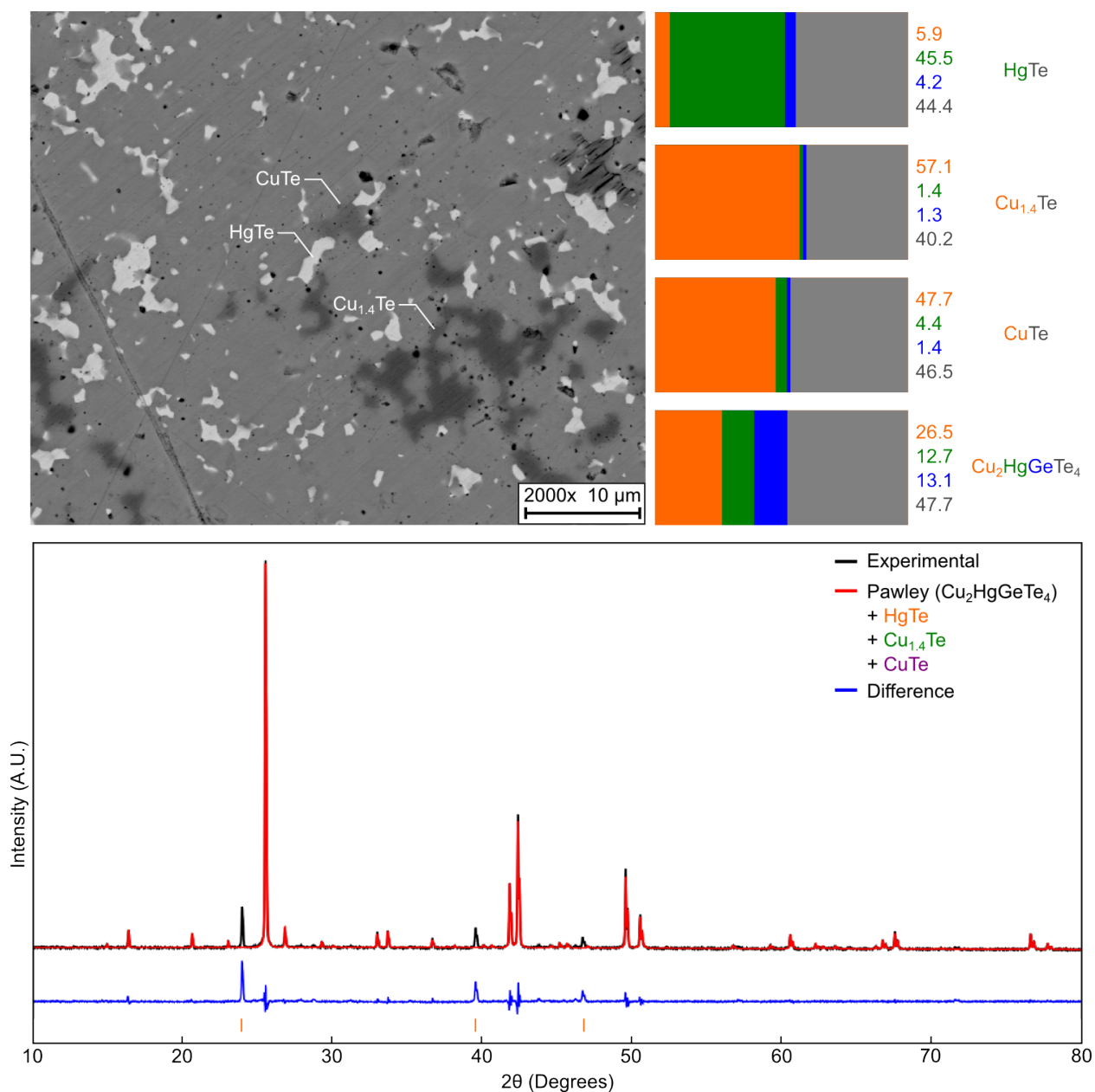


Figure S4: X-ray diffraction (XRD), scanning electron microscopy (SEM), and energy dispersive spectroscopy (EDS) characterization for the HgTe-Cu_{1.4}Te-CuTe-Cu₂HgGeTe₄ critical point. For XRD, a Pawley analysis is performed to assess the lattice parameters of the Cu₂HgGeTe₄ matrix phase. SEM image is a typical backscatter electron image of the densified pellet. The EDS analysis represents an average composition for each of the impurity phases and the Cu₂HgGeTe₄ matrix phase. EDS was performed and averaged over multiple precipitates (~ 5) for impurities and multiple locations within the matrix phase (~ 10). This is one case where XRD is unreliable and fails to identify Cu_{1.4}Te and CuTe even though they are quite obvious through SEM.

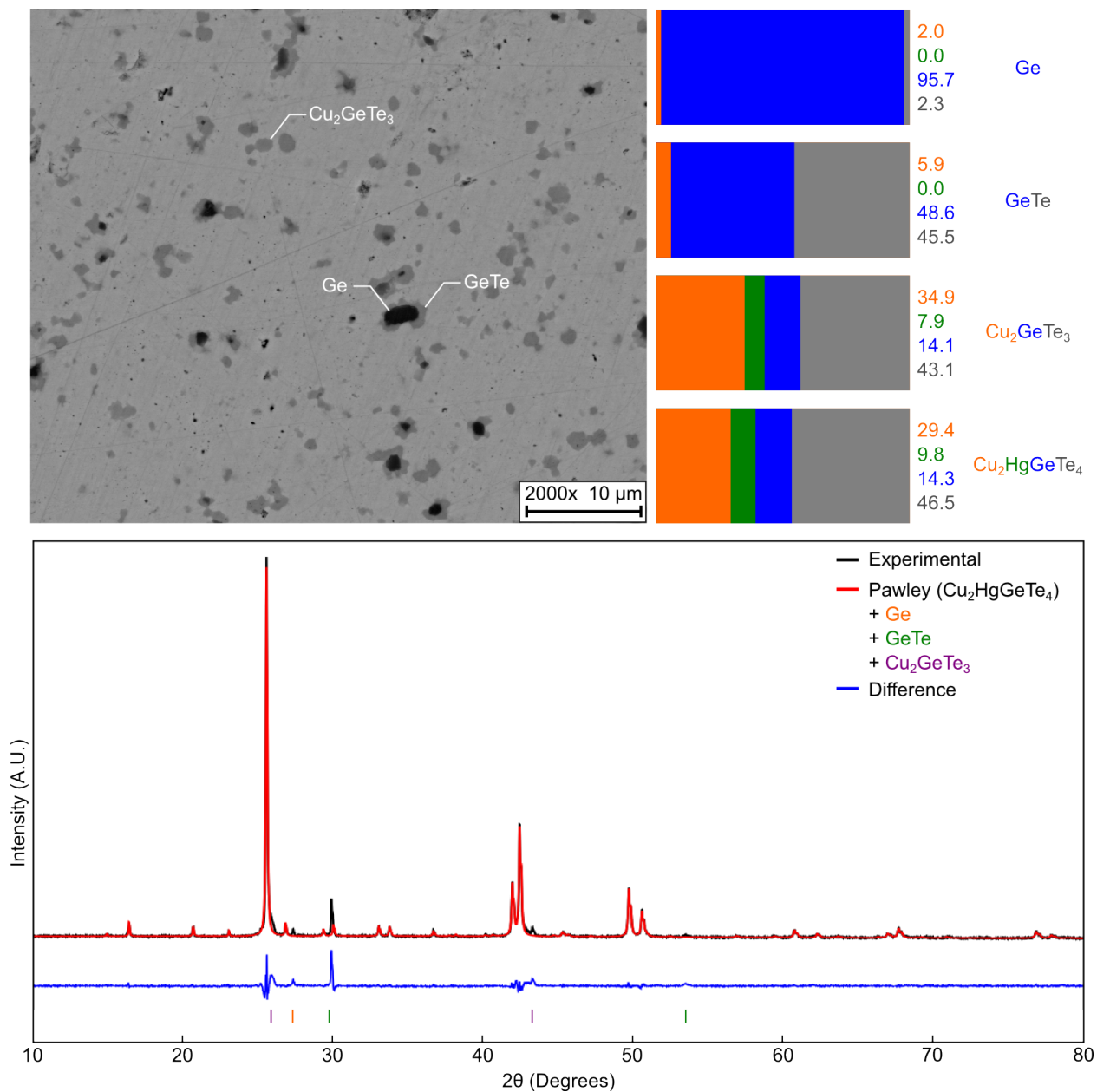


Figure S5: X-ray diffraction (XRD), scanning electron microscopy (SEM), and energy dispersive spectroscopy (EDS) characterization for the Ge-GeTe-Cu₂GeTe₃-Cu₂HgGeTe₄ critical point. For XRD, a Pawley analysis is performed to assess the lattice parameters of the Cu₂HgGeTe₄ matrix phase. SEM image is a typical backscatter electron image of the den-sified pellet. The EDS analysis represents an average composition for each of the impurity phases and the Cu₂HgGeTe₄ matrix phase. EDS was performed and averaged over multiple precipitates (~ 5) for impurities and multiple locations within the matrix phase (~ 10).

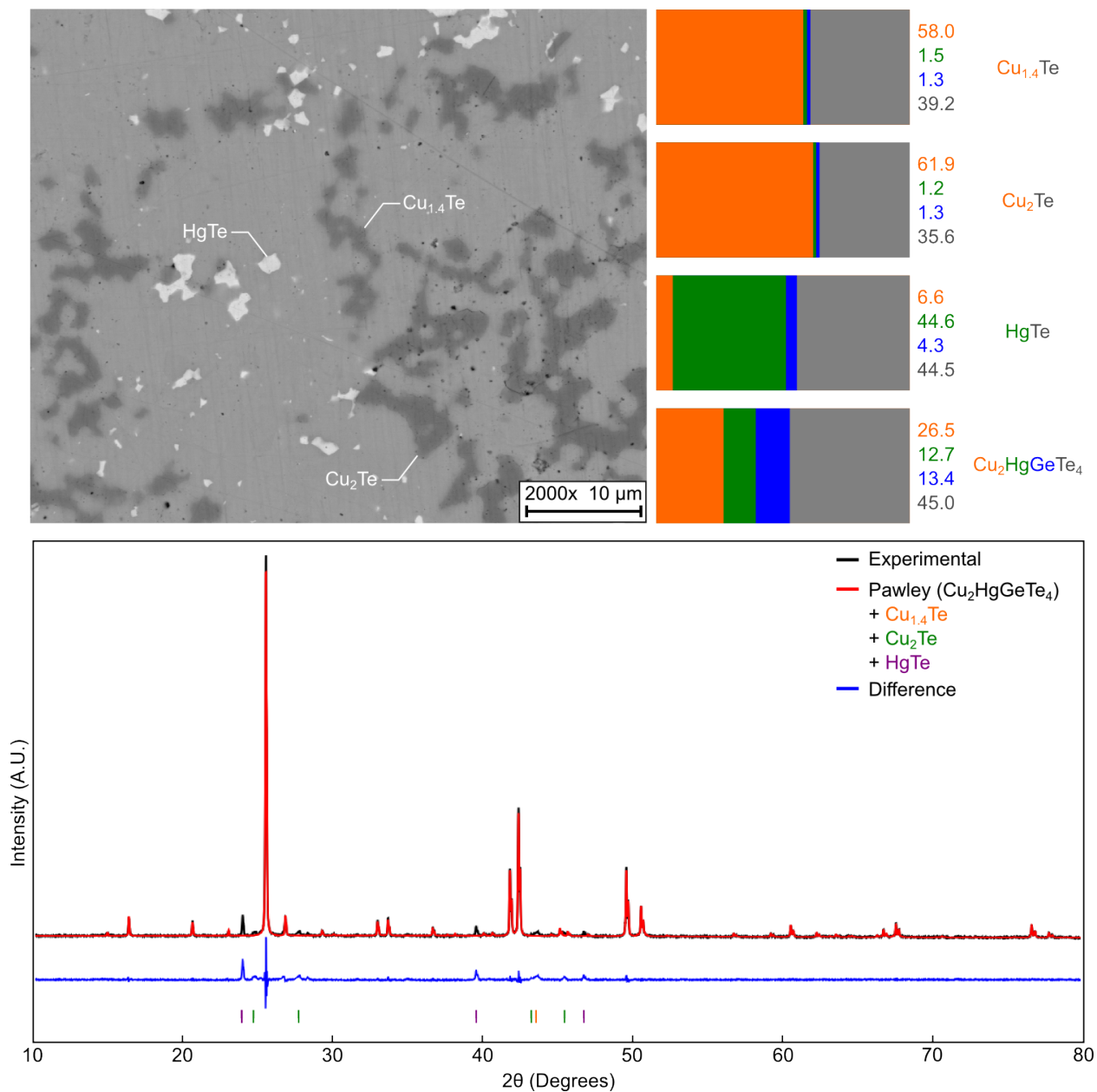


Figure S6: X-ray diffraction (XRD), scanning electron microscopy (SEM), and energy dispersive spectroscopy (EDS) characterization for the Cu_{1.4}Te-Cu₂Te-HgTe-Cu₂HgGeTe₄ critical point. For XRD, a Pawley analysis is performed to assess the lattice parameters of the Cu₂HgGeTe₄ matrix phase. SEM image is a typical backscatter electron image of the den-sified pellet. The EDS analysis represents an average composition for each of the impurity phases and the Cu₂HgGeTe₄ matrix phase. EDS was performed and averaged over multiple precipitates (~ 5) for impurities and multiple locations within the matrix phase (~ 10).

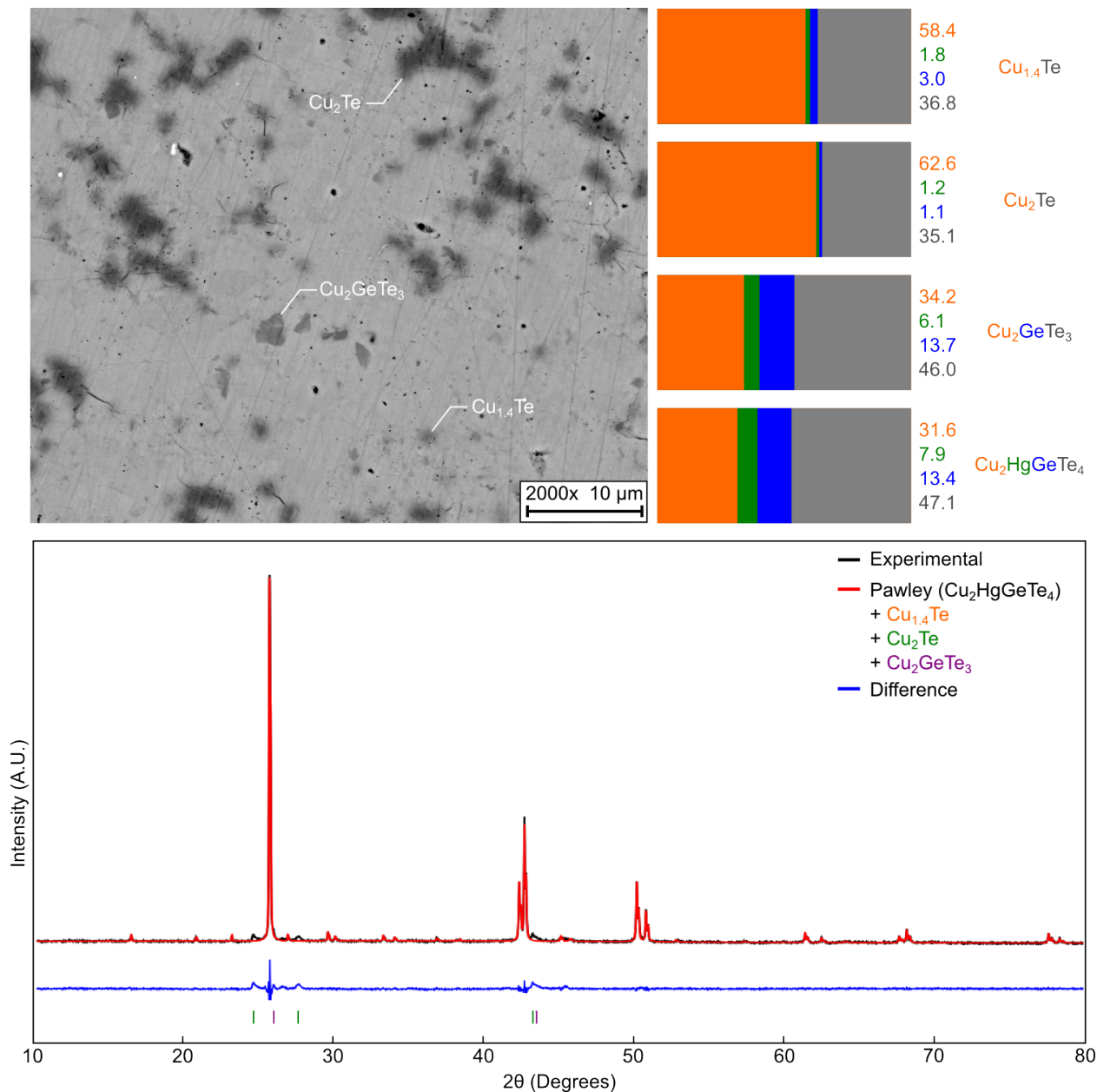


Figure S7: X-ray diffraction (XRD), scanning electron microscopy (SEM), and energy dispersive spectroscopy (EDS) characterization for the $\text{Cu}_{1.4}\text{Te}$ - Cu_2Te - Cu_2GeTe_3 - $\text{Cu}_2\text{HgGeTe}_4$ critical point. For XRD, a Pawley analysis is performed to assess the lattice parameters of the $\text{Cu}_2\text{HgGeTe}_4$ matrix phase. SEM image is a typical backscatter electron image of the densified pellet. Small cracks on surface are caused by polishing and do not appear in fracture surface images. The EDS analysis represents an average composition for each of the impurity phases and the $\text{Cu}_2\text{HgGeTe}_4$ matrix phase. EDS was performed and averaged over multiple precipitates (~ 5) for impurities and multiple locations within the matrix phase (~ 10). XRD fails to identify $\text{Cu}_{1.4}\text{Te}$, which is expected based on the low concentrations observed in SEM.

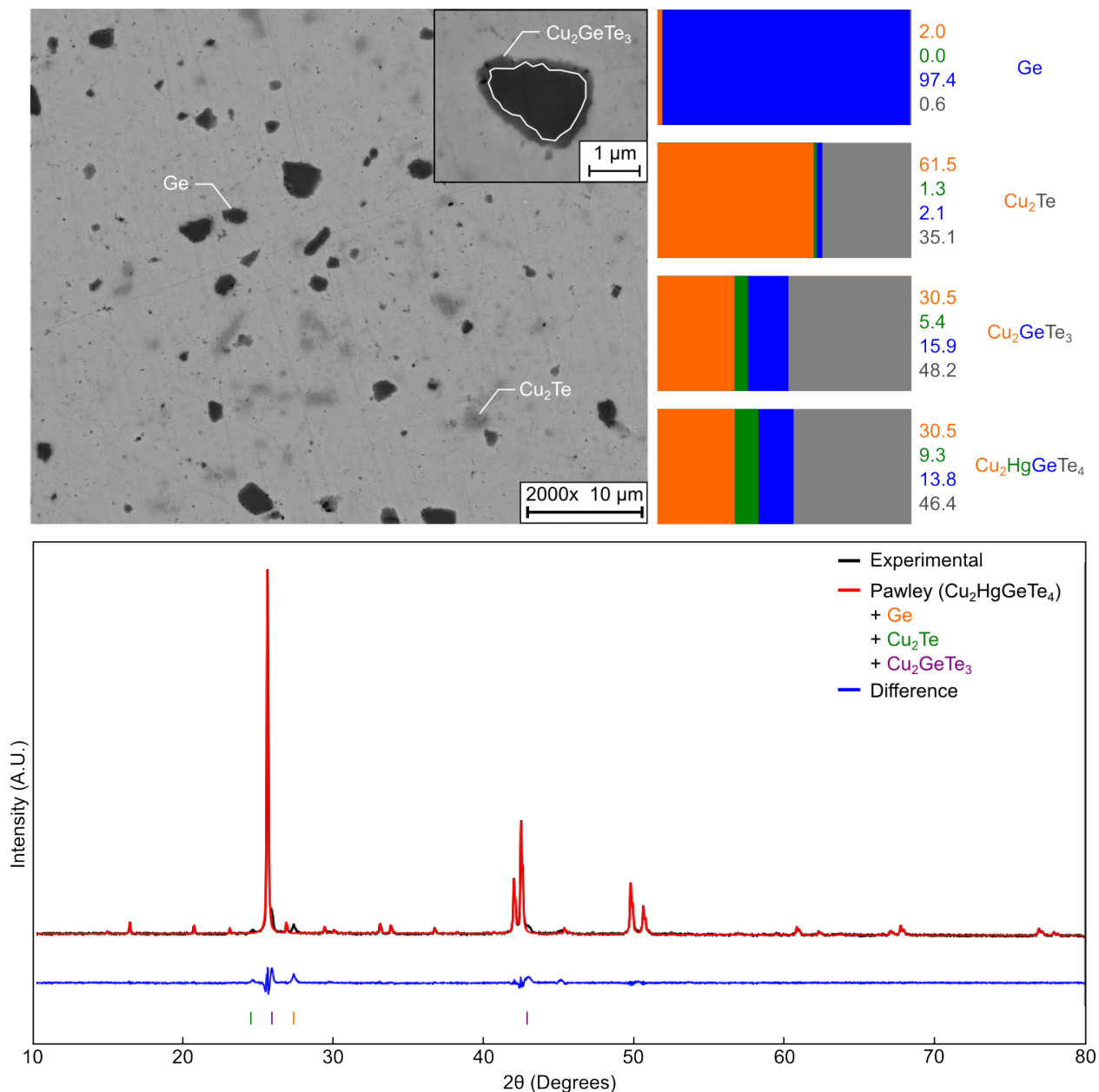


Figure S8: X-ray diffraction (XRD), scanning electron microscopy (SEM), and energy dispersive spectroscopy (EDS) characterization for the Ge-Cu₂Te-Cu₂GeTe₃-Cu₂HgGeTe₄ critical point. For XRD, a Pawley analysis is performed to assess the lattice parameters of the Cu₂HgGeTe₄ matrix phase. SEM image is a typical backscatter electron image of the densified pellet. In this region, we observe Cu₂GeTe₃ as a shell around the Ge precipitates (inset). The EDS analysis represents an average composition for each of the impurity phases and the Cu₂HgGeTe₄ matrix phase. EDS was performed and averaged over multiple precipitates (~5) for impurities and multiple locations within the matrix phase (~10).

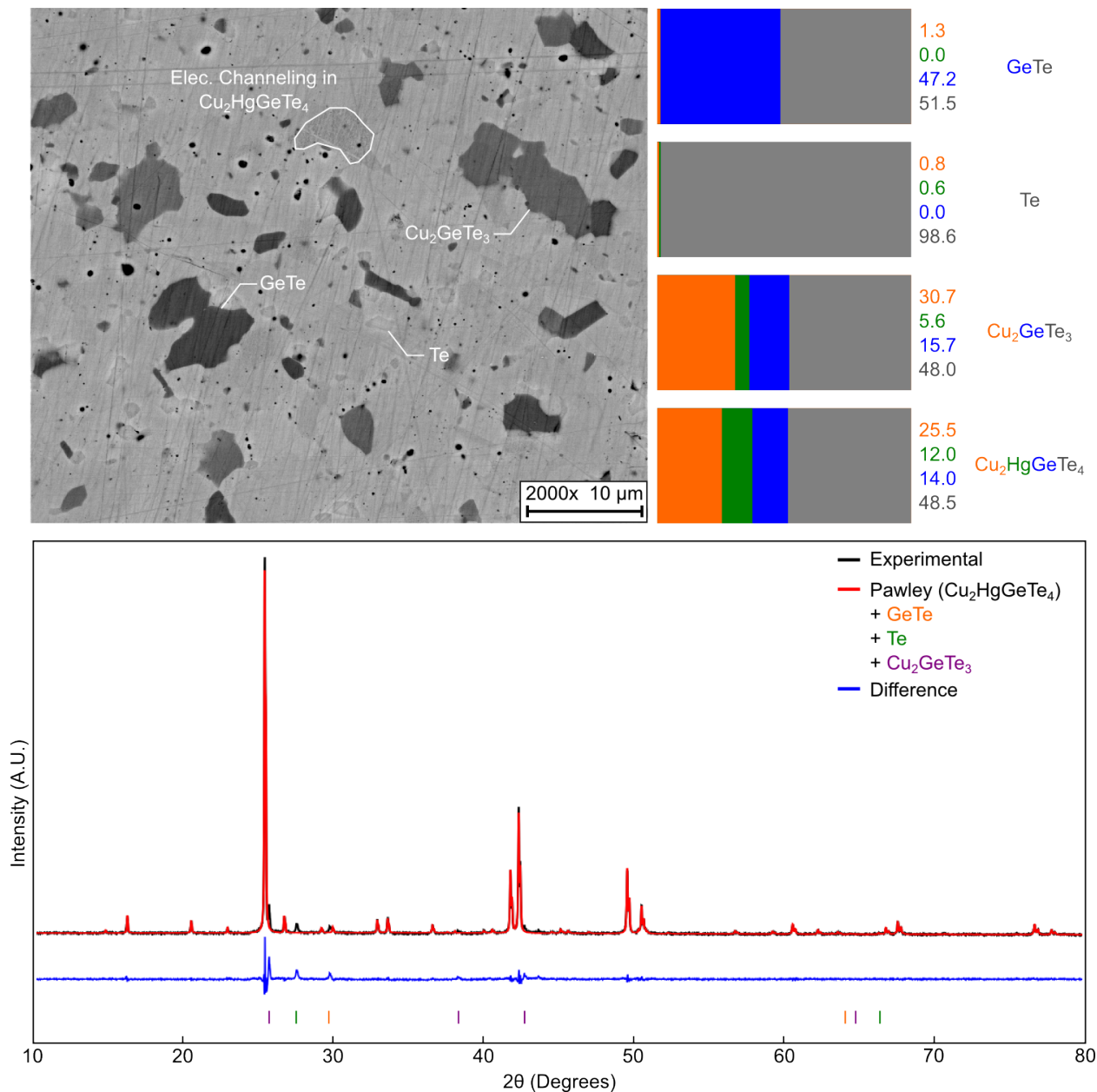


Figure S9: X-ray diffraction (XRD), scanning electron microscopy (SEM), and energy dispersive spectroscopy (EDS) characterization for the $\text{GeTe-Te-Cu}_2\text{GeTe}_3\text{-Cu}_2\text{HgGeTe}_4$ critical point. For XRD, a Pawley analysis is performed to assess the lattice parameters of the $\text{Cu}_2\text{HgGeTe}_4$ matrix phase. SEM image is a typical backscatter electron image of the densified pellet. In this region, we observe grains of $\text{Cu}_2\text{HgGeTe}_4$ that exhibit contrast in backscatter due to electron channeling (highlighted). EDS analysis indicates that these grains are identical to $\text{Cu}_2\text{HgGeTe}_4$ composition. The EDS analysis represents an average composition for each of the impurity phases and the $\text{Cu}_2\text{HgGeTe}_4$ matrix phase. EDS was performed and averaged over multiple precipitates (~ 5) for impurities and multiple locations within the matrix phase (~ 10).

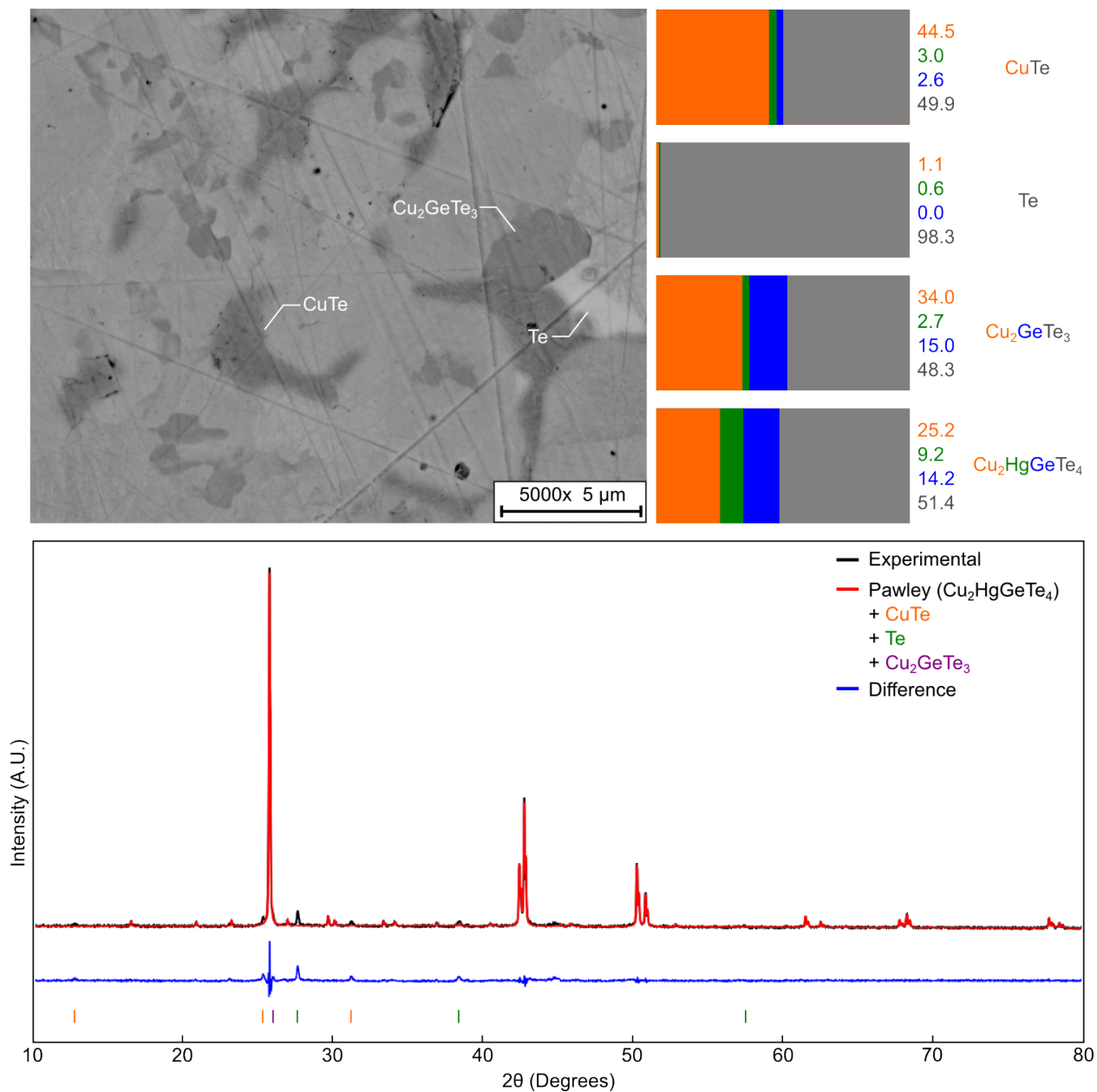


Figure S10: X-ray diffraction (XRD), scanning electron microscopy (SEM), and energy dispersive spectroscopy (EDS) characterization for the CuTe-Te-Cu₂GeTe₃-Cu₂HgGeTe₄ critical point. For XRD, a Pawley analysis is performed to assess the lattice parameters of the Cu₂HgGeTe₄ matrix phase. SEM image is a typical backscatter electron image of the den-sified pellet. The EDS analysis represents an average composition for each of the impurity phases and the Cu₂HgGeTe₄ matrix phase. EDS was performed and averaged over multiple precipitates (~ 5) for impurities and multiple locations within the matrix phase (~ 10).

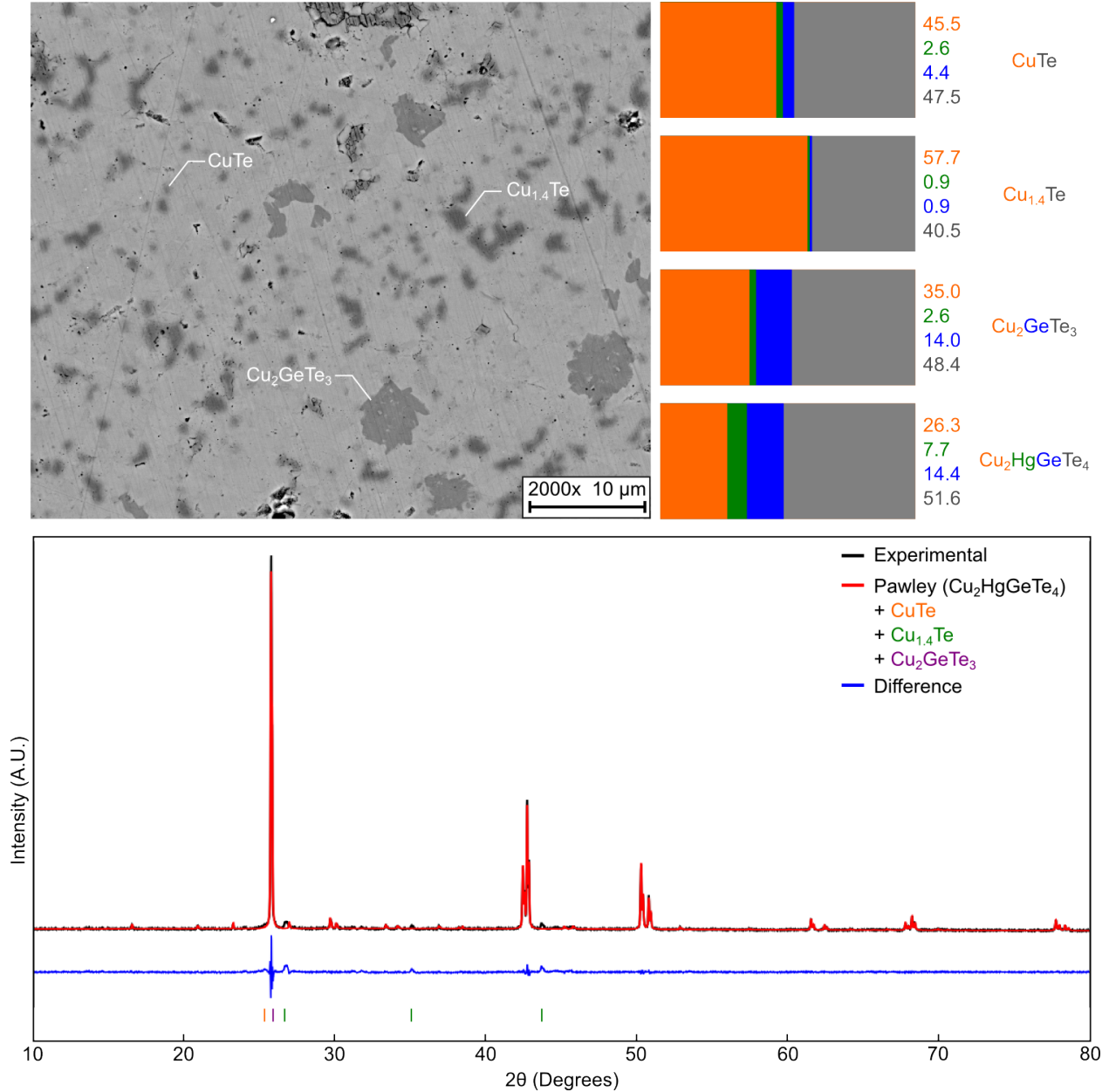


Figure S11: X-ray diffraction (XRD), scanning electron microscopy (SEM), and energy dispersive spectroscopy (EDS) characterization for the CuTe-Cu_{1.4}Te-Cu₂GeTe₃-Cu₂HgGeTe₄ critical point. For XRD, a Pawley analysis is performed to assess the lattice parameters of the Cu₂HgGeTe₄ matrix phase. SEM image is a typical backscatter electron image of the densified pellet. We observe some liftout of Cu_{1.4}Te grains during polishing. The EDS analysis represents an average composition for each of the impurity phases and the Cu₂HgGeTe₄ matrix phase. EDS was performed and averaged over multiple precipitates (~5) for impurities and multiple locations within the matrix phase (~10).

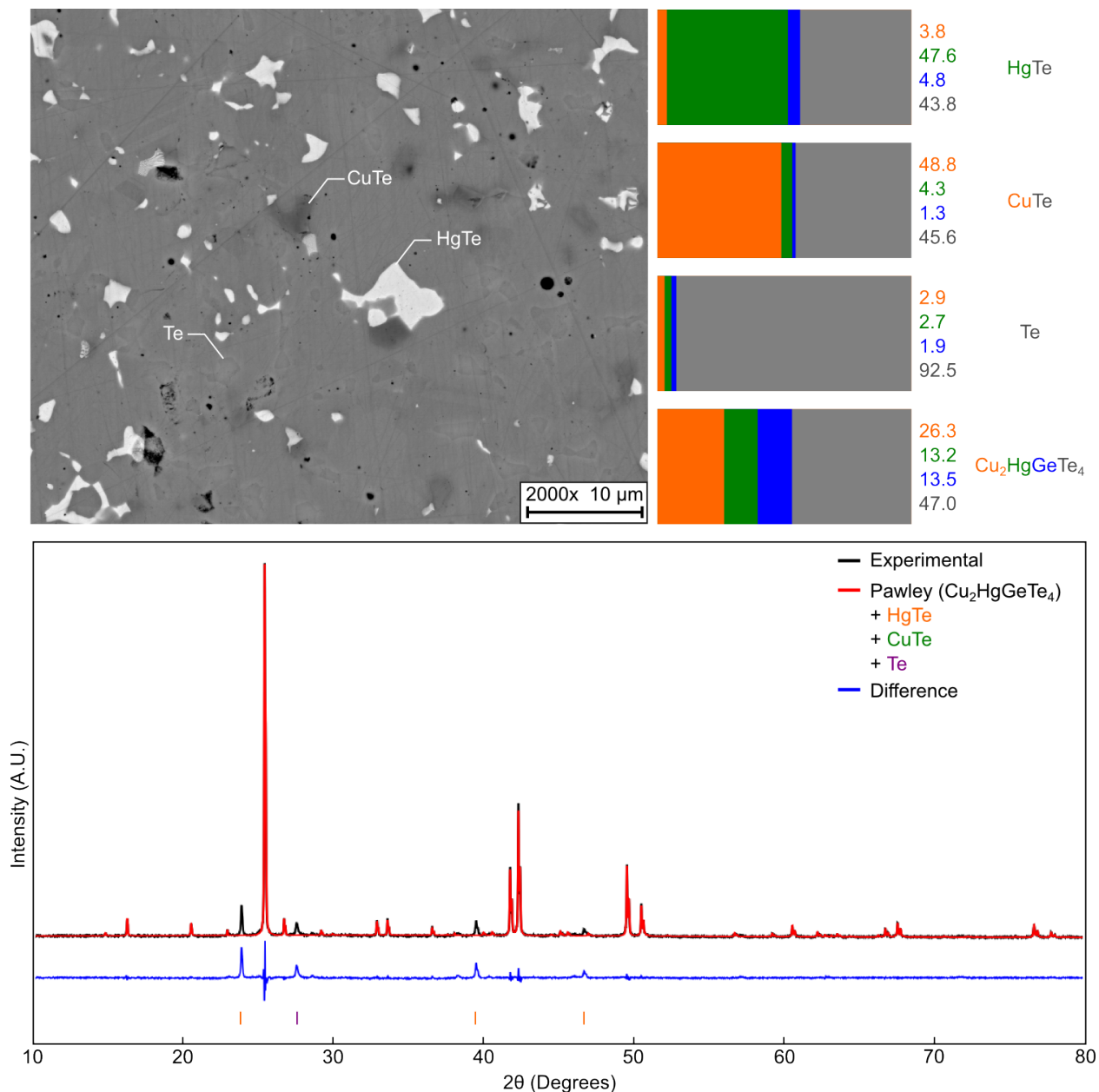


Figure S12: X-ray diffraction (XRD), scanning electron microscopy (SEM), and energy dispersive spectroscopy (EDS) characterization for the HgTe-CuTe-Te-Cu₂HgGeTe₄ critical point. For XRD, a Pawley analysis is performed to assess the lattice parameters of the Cu₂HgGeTe₄ matrix phase. SEM image is a typical backscatter electron image of the densified pellet. The EDS analysis represents an average composition for each of the impurity phases and the Cu₂HgGeTe₄ matrix phase. EDS was performed and averaged over multiple precipitates (~5) for impurities and multiple locations within the matrix phase (~10). XRD fails to identify CuTe, although this is expected with the low concentration observed in SEM.

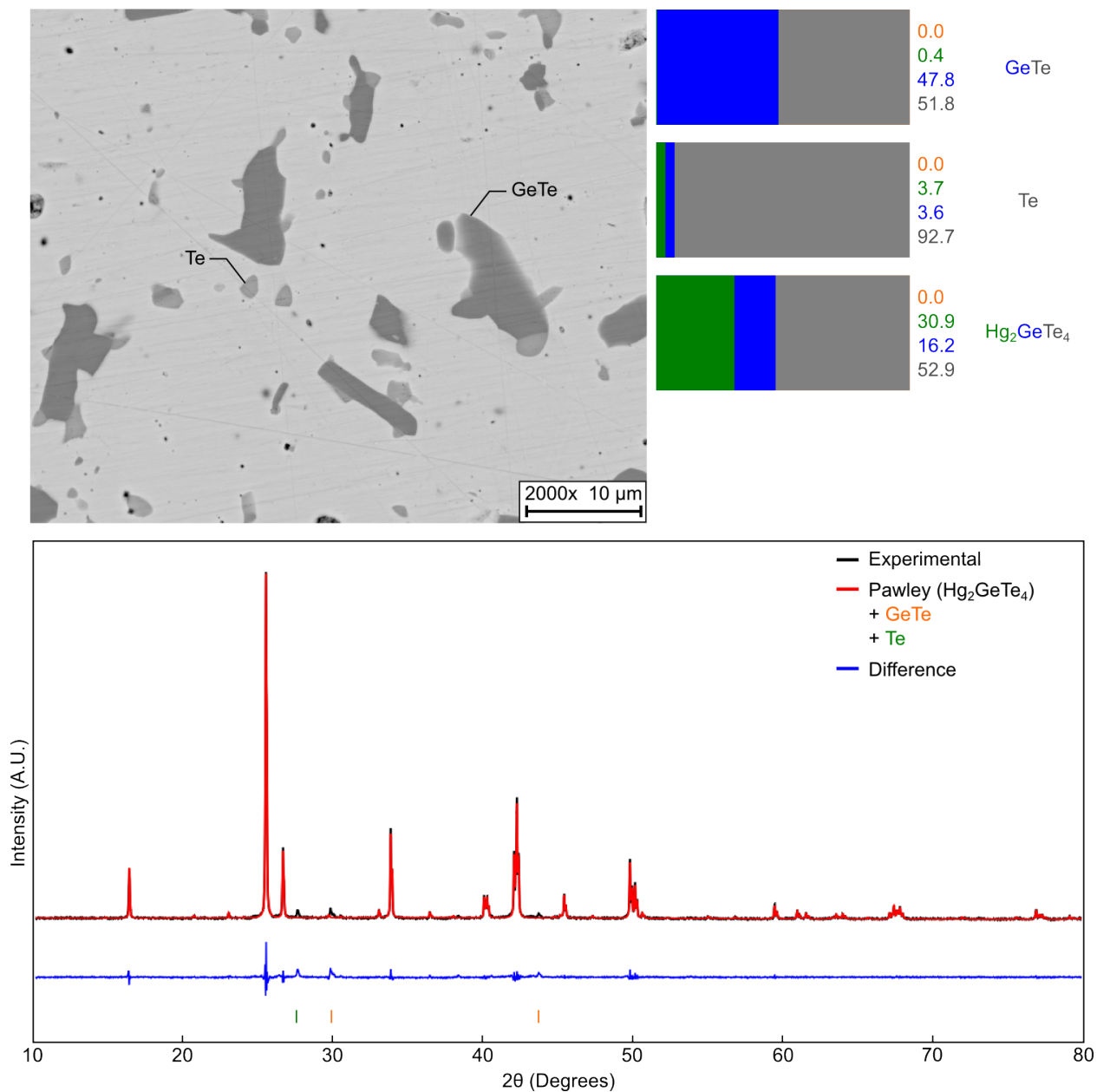


Figure S13: X-ray diffraction (XRD), scanning electron microscopy (SEM), and energy dispersive spectroscopy (EDS) characterization for the GeTe-Te-Hg₂GeTe₄ critical point. For XRD, a Pawley analysis is performed to assess the lattice parameters of the Hg₂GeTe₄ matrix phase. SEM image is a typical backscatter electron image of the densified pellet. The EDS analysis represents an average composition for each of the impurity phases and the Hg₂GeTe₄ matrix phase. EDS was performed and averaged over multiple precipitates (~5) for impurities and multiple locations within the matrix phase (~10).

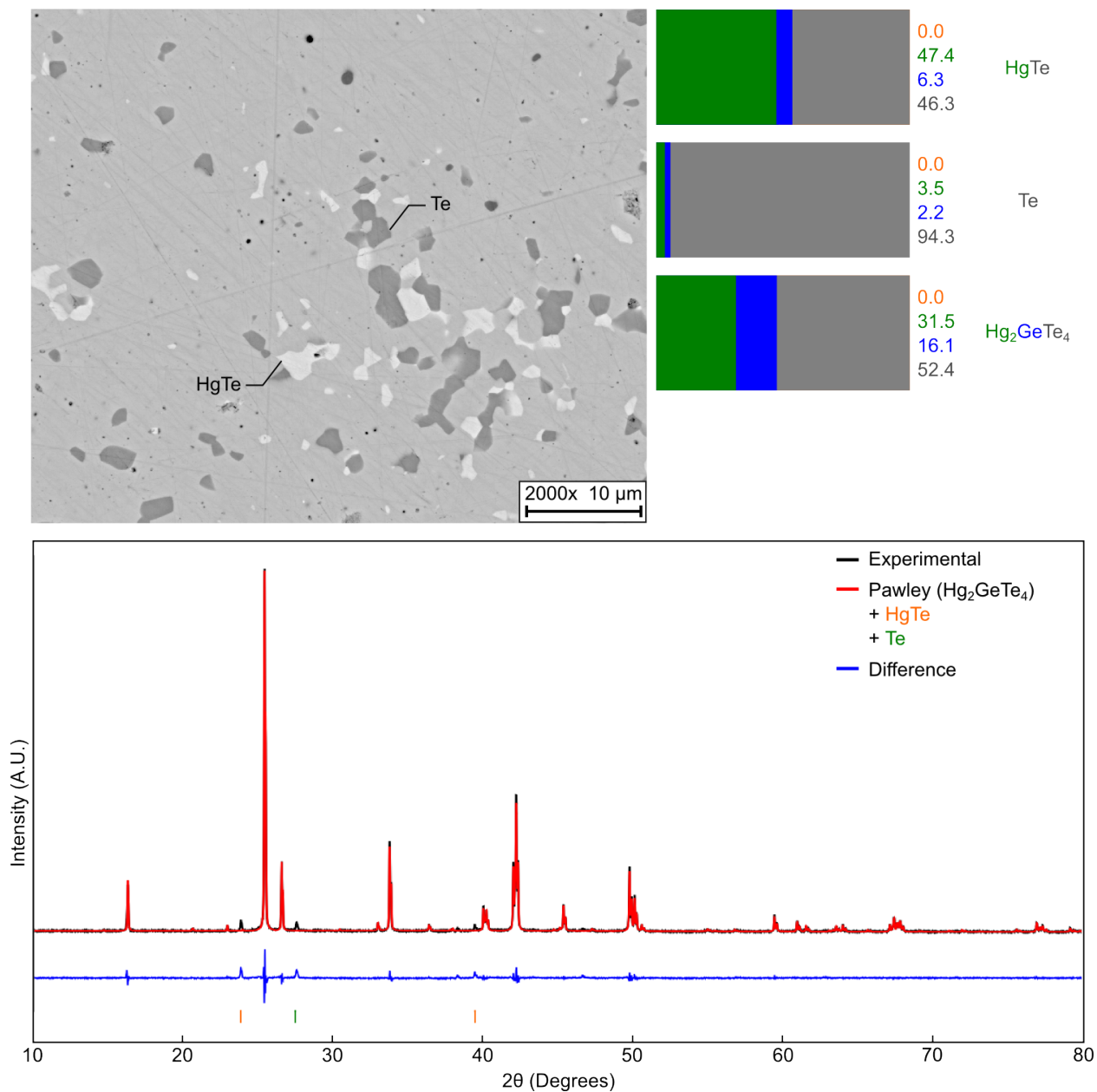


Figure S14: X-ray diffraction (XRD), scanning electron microscopy (SEM), and energy dispersive spectroscopy (EDS) characterization for the HgTe-Te-Hg₂GeTe₄ critical point. For XRD, a Pawley analysis is performed to assess the lattice parameters of the Hg₂GeTe₄ matrix phase. SEM image is a typical backscatter electron image of the densified pellet. The EDS analysis represents an average composition for each of the impurity phases and the Hg₂GeTe₄ matrix phase. EDS was performed and averaged over multiple precipitates (~5) for impurities and multiple locations within the matrix phase (~10).

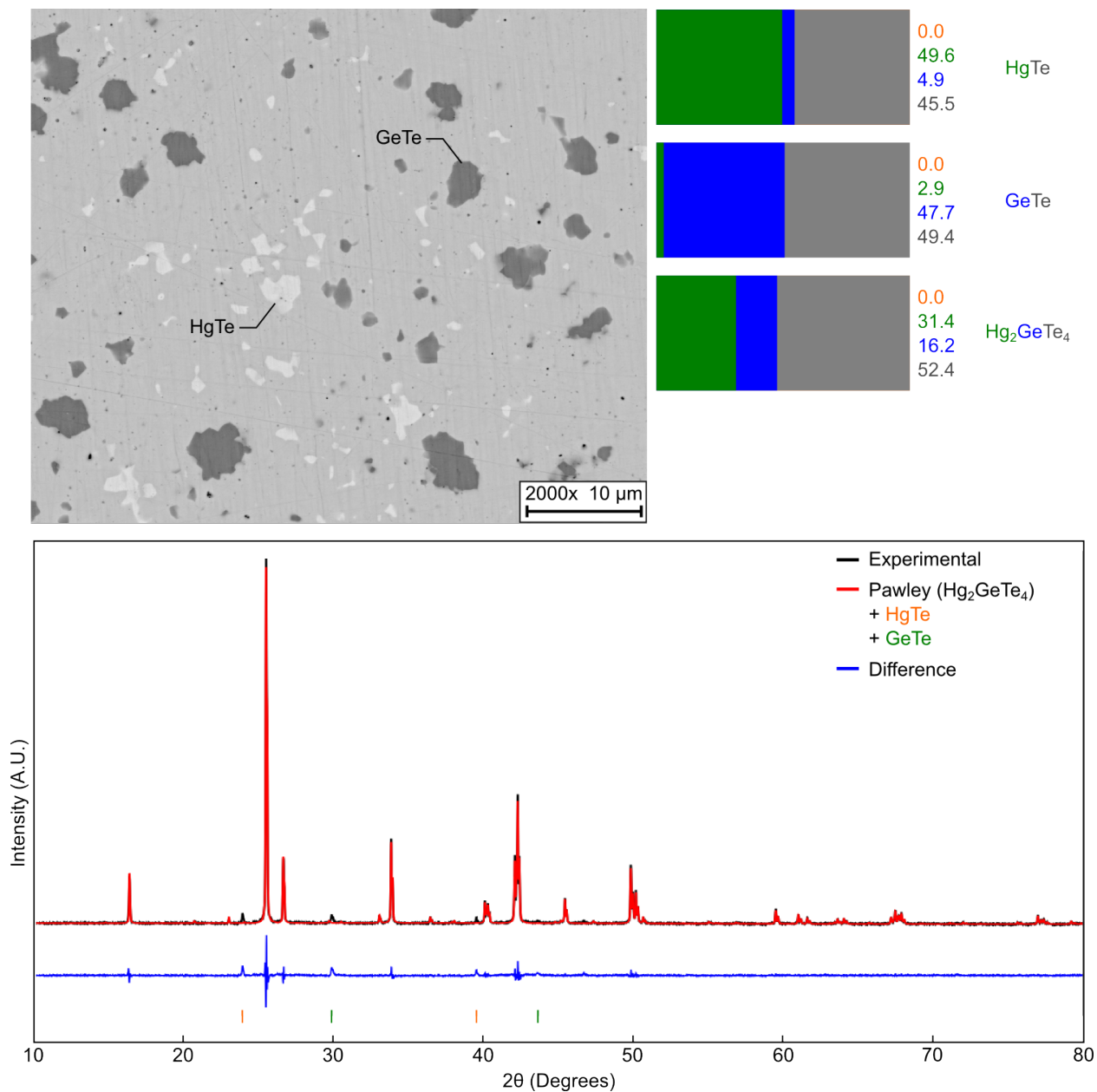


Figure S15: X-ray diffraction (XRD), scanning electron microscopy (SEM), and energy dispersive spectroscopy (EDS) characterization for the HgTe-GeTe-Hg₂GeTe₄ critical point. For XRD, a Pawley analysis is performed to assess the lattice parameters of the Hg₂GeTe₄ matrix phase. SEM image is a typical backscatter electron image of the densified pellet. The EDS analysis represents an average composition for each of the impurity phases and the Hg₂GeTe₄ matrix phase. EDS was performed and averaged over multiple precipitates (~5) for impurities and multiple locations within the matrix phase (~10).

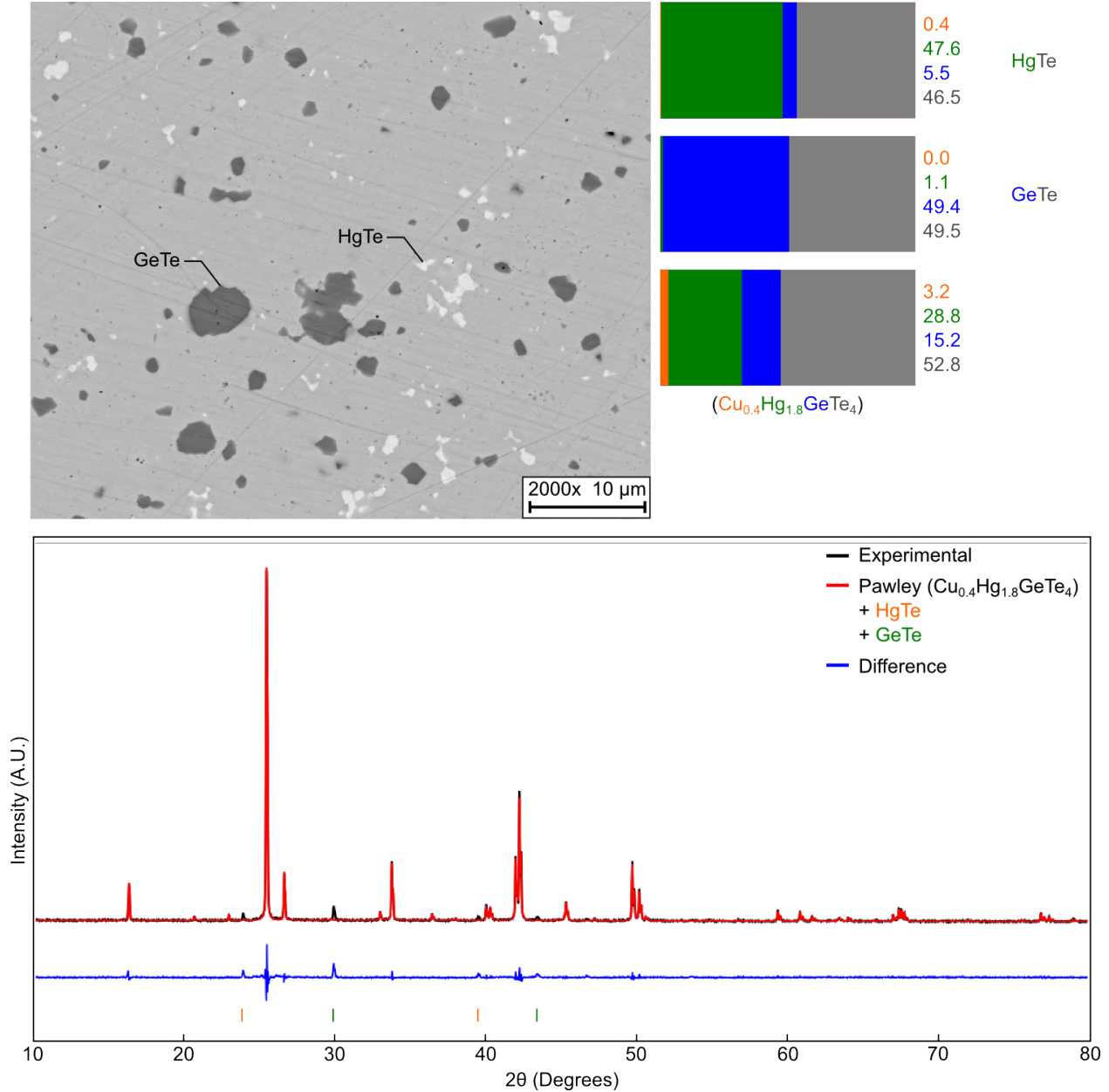


Figure S16: X-ray diffraction (XRD), scanning electron microscopy (SEM), and energy dispersive spectroscopy (EDS) characterization for the $\text{Cu}_{2x}\text{Hg}_{2-x}\text{GeTe}_4$ alloy ($x = 0.2$). Impurities of GeTe and HgTe serve to tie sample to the same edge of the alloy single-phase region. For XRD, a Pawley analysis is performed to assess the lattice parameters of the Hg_2GeTe_4 matrix phase. SEM image is a typical backscatter electron image of the densified pellet. The EDS analysis represents an average composition for each of the impurity phases and the alloyed matrix phase. EDS was performed and averaged over multiple precipitates (~ 5) for impurities and multiple locations within the matrix phase (~ 10).

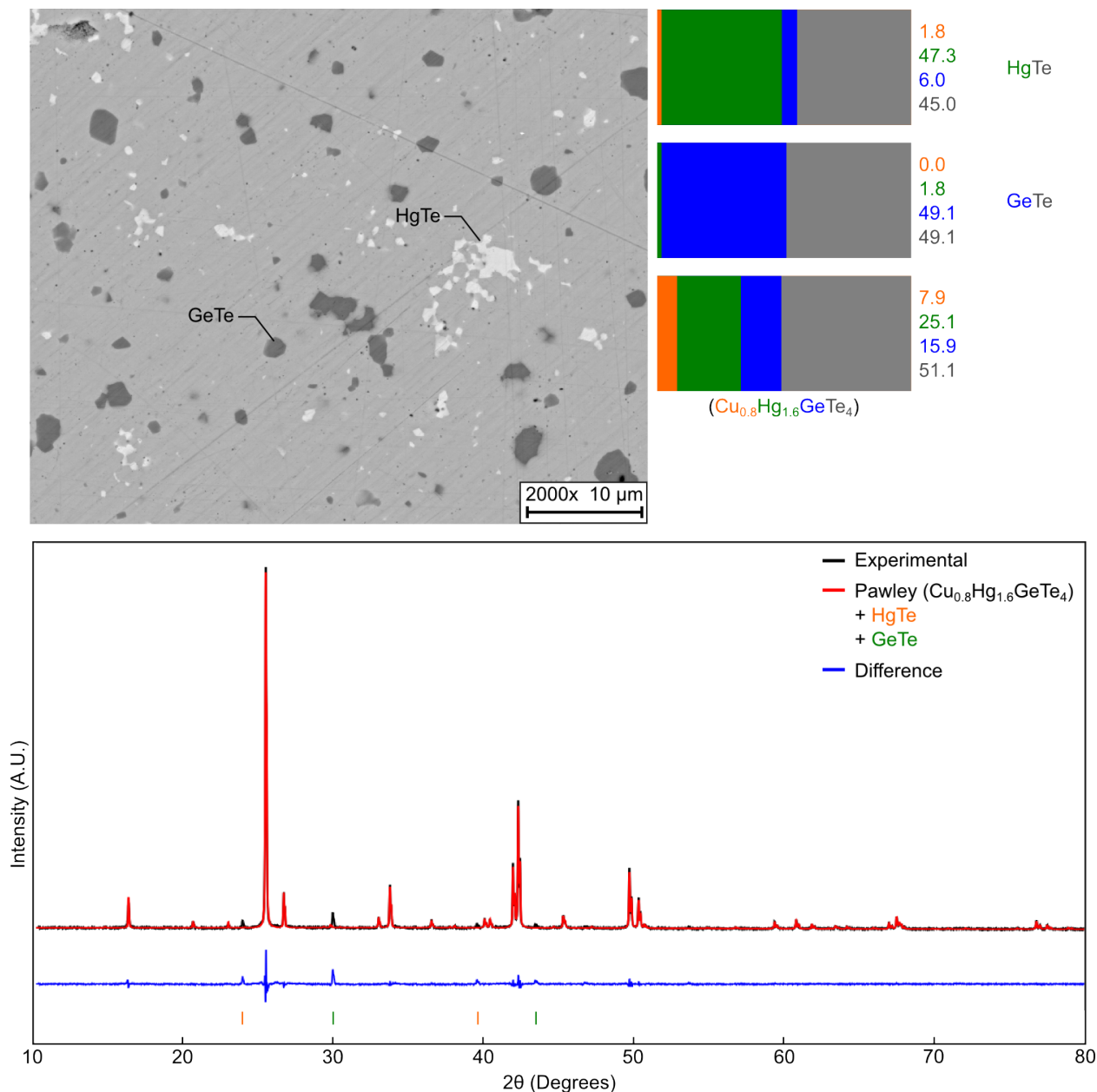


Figure S17: X-ray diffraction (XRD), scanning electron microscopy (SEM), and energy dispersive spectroscopy (EDS) characterization for the $\text{Cu}_{2x}\text{Hg}_{2-x}\text{GeTe}_4$ alloy ($x = 0.4$). Impurities of GeTe and HgTe serve to tie sample to the same edge of the alloy single-phase region. For XRD, a Pawley analysis is performed to assess the lattice parameters of the Hg_2GeTe_4 matrix phase. SEM image is a typical backscatter electron image of the densified pellet. The EDS analysis represents an average composition for each of the impurity phases and the alloyed matrix phase. EDS was performed and averaged over multiple precipitates (~ 5) for impurities and multiple locations within the matrix phase (~ 10).

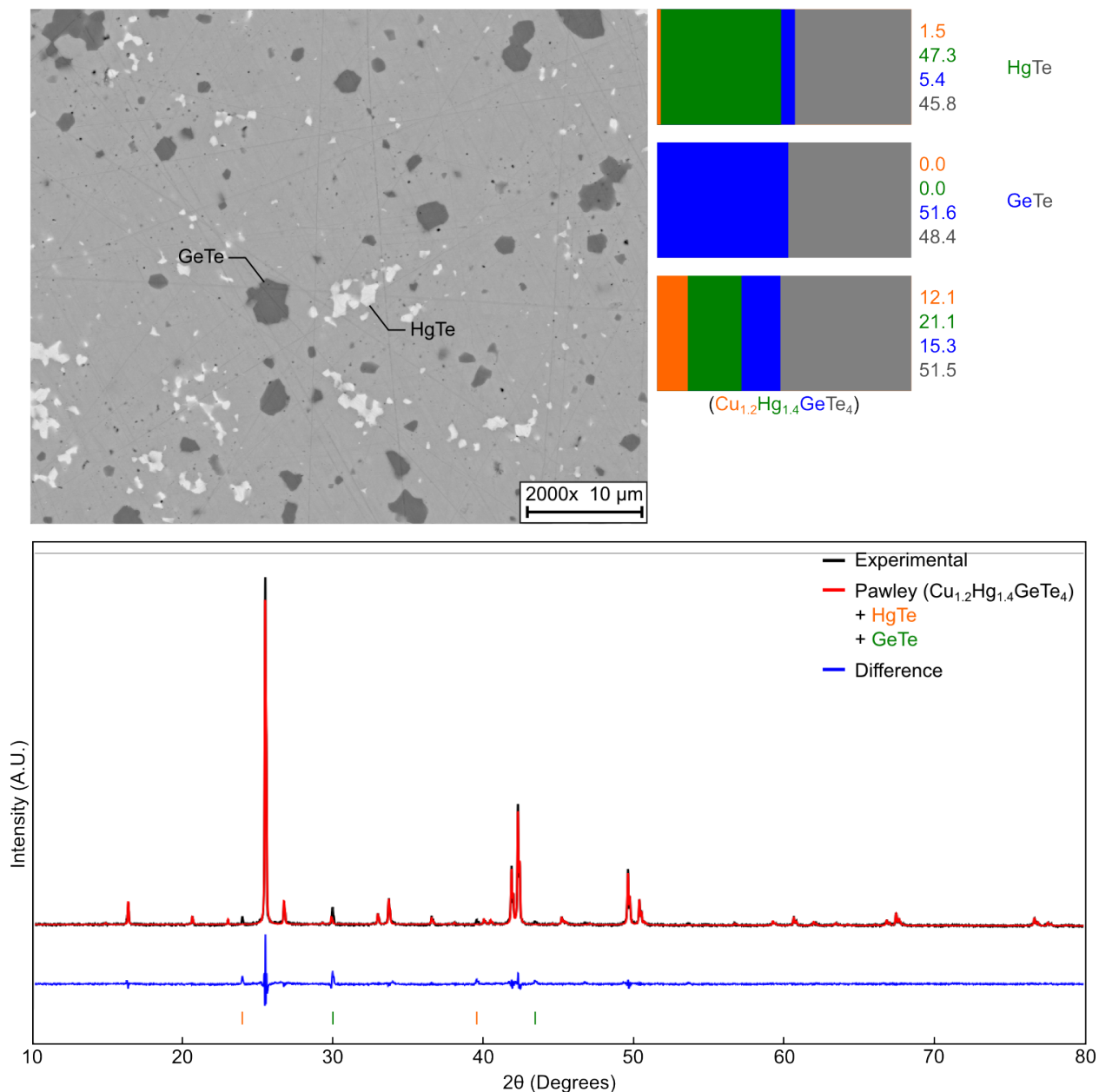


Figure S18: X-ray diffraction (XRD), scanning electron microscopy (SEM), and energy dispersive spectroscopy (EDS) characterization for the $\text{Cu}_{2x}\text{Hg}_{2-x}\text{GeTe}_4$ alloy ($x = 0.6$). Impurities of GeTe and HgTe serve to tie sample to the same edge of the alloy single-phase region. For XRD, a Pawley analysis is performed to assess the lattice parameters of the Hg_2GeTe_4 matrix phase. SEM image is a typical backscatter electron image of the densified pellet. The EDS analysis represents an average composition for each of the impurity phases and the alloyed matrix phase. EDS was performed and averaged over multiple precipitates (~ 5) for impurities and multiple locations within the matrix phase (~ 10).

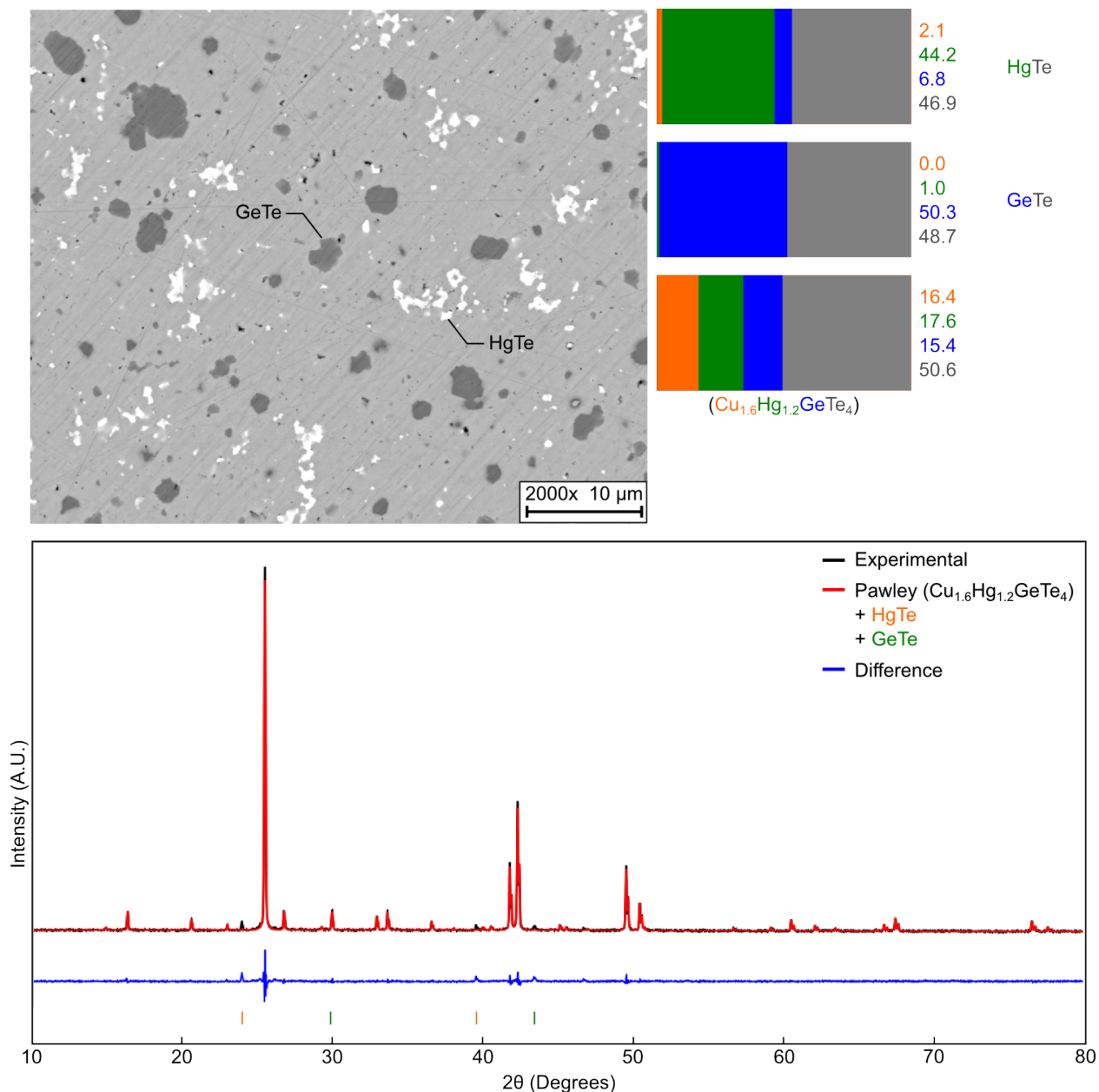


Figure S19: X-ray diffraction (XRD), scanning electron microscopy (SEM), and energy dispersive spectroscopy (EDS) characterization for the $\text{Cu}_{2x}\text{Hg}_{2-x}\text{GeTe}_4$ alloy ($x = 0.8$). Impurities of GeTe and HgTe serve to tie sample to the same edge of the alloy single-phase region. For XRD, a Pawley analysis is performed to assess the lattice parameters of the Hg_2GeTe_4 matrix phase. SEM image is a typical backscatter electron image of the densified pellet. The EDS analysis represents an average composition for each of the impurity phases and the alloyed matrix phase. EDS was performed and averaged over multiple precipitates (~ 5) for impurities and multiple locations within the matrix phase (~ 10).

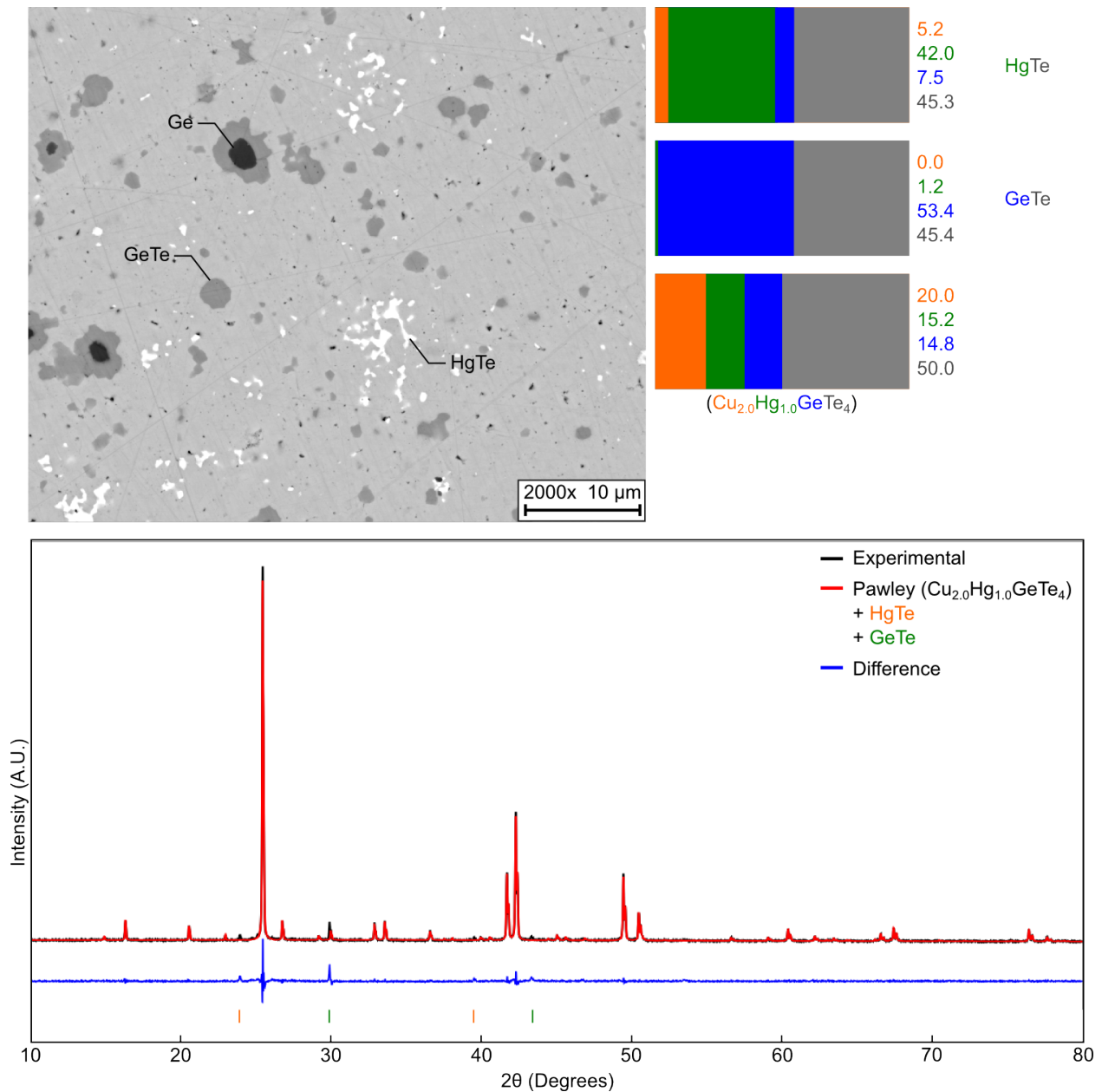


Figure S20: X-ray diffraction (XRD), scanning electron microscopy (SEM), and energy dispersive spectroscopy (EDS) characterization for the $\text{Cu}_{2x}\text{Hg}_{2-x}\text{GeTe}_4$ alloy ($x = 1.0$). Impurities of GeTe and HgTe serve to tie sample to the same edge of the alloy single-phase region. The emergence of Ge in this sample is expected, as the sample composition at $x = 1.0$ is actually within a proper four-phase critical point ($\text{Ge-HgTe-GeTe-Cu}_2\text{HgGeTe}_4$). For XRD, a Pawley analysis is performed to assess the lattice parameters of the Hg_2GeTe_4 matrix phase. SEM image is a typical back backscatter image of the densified pellet. The EDS analysis represents an average composition for each of the impurity phases and the alloyed matrix phase. EDS was performed and averaged over multiple precipitates (~ 5) for impurities and multiple locations within the matrix phase (~ 10).

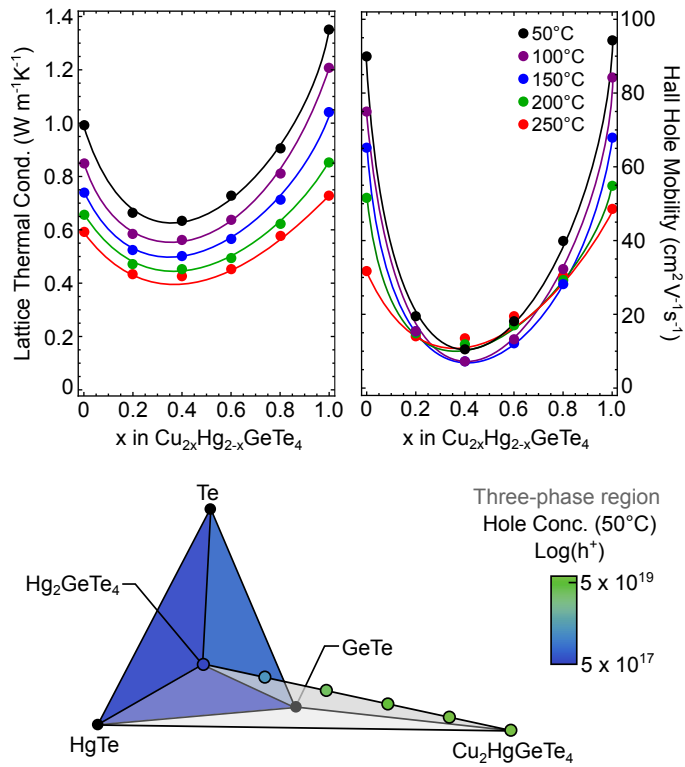


Figure S21: In both the lattice thermal conductivity and the Hall mobility, we see strong evidence of alloy scattering along the Hg_2GeTe_4 - $\text{Cu}_2\text{HgGeTe}_4$ alloys. As the alloy compositions must include a large degree of site disorder with incremental Cu addition, the Hall mobility is particularly disrupted by the alloying.

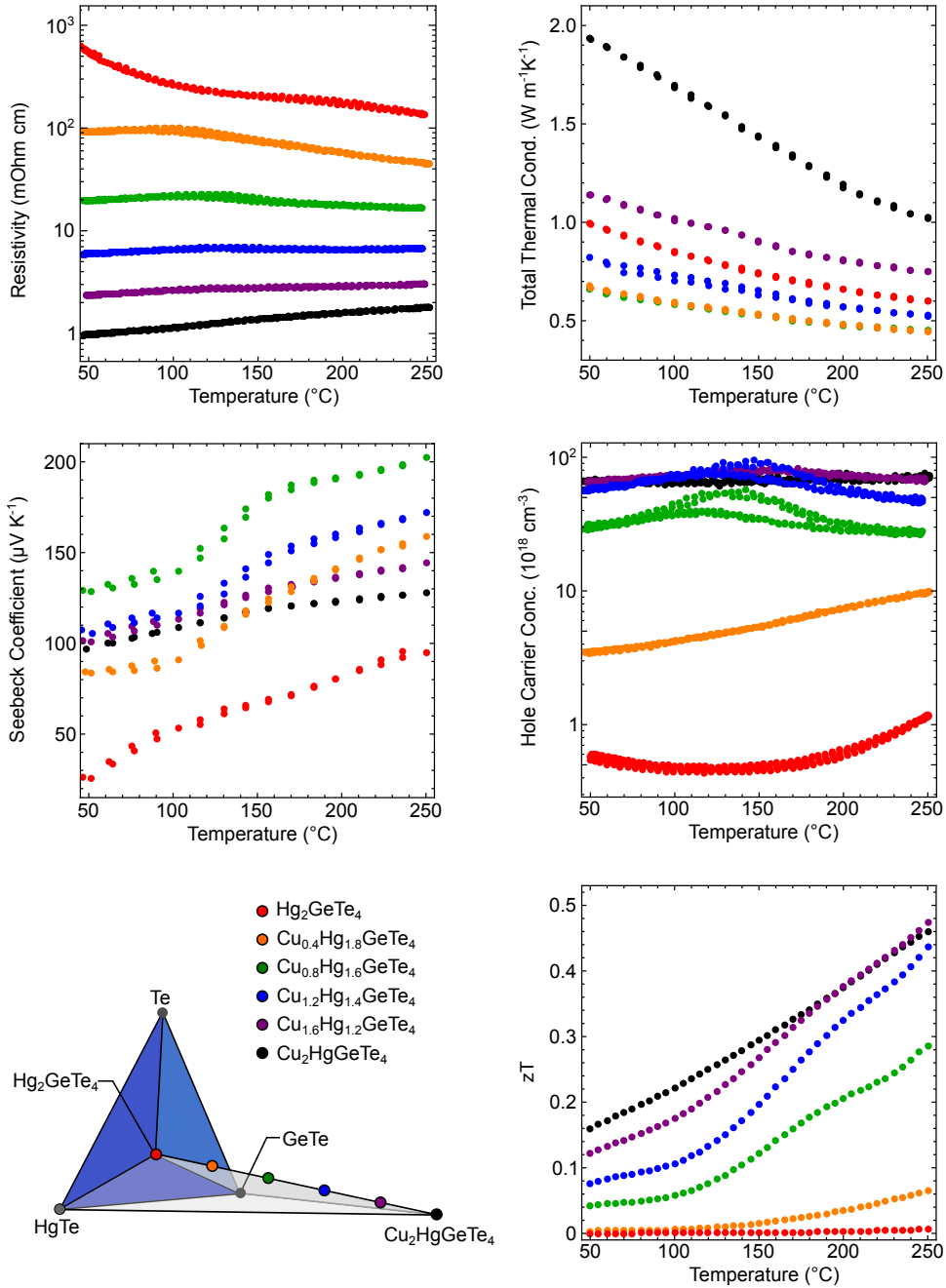


Figure S22: A full suite of thermoelectric transport measurements along the Hg_2GeTe_4 - $\text{Cu}_2\text{HgGeTe}_4$ alloys demonstrates transport consistent with an alloy between an intrinsic (Hg_2GeTe_4) and degenerate ($\text{Cu}_2\text{HgGeTe}_4$) semiconductor. While it is possible to optimize the p-type carrier concentration through the Hg_2GeTe_4 - $\text{Cu}_2\text{HgGeTe}_4$ alloy series, it is likely undesirable due to the increased alloy scattering in the electronic conductivity and mobility (see Figure S21). As such, the values for zT along the alloying line may not be representative of the optimized properties of either Hg_2GeTe_4 or $\text{Cu}_2\text{HgGeTe}_4$.